Lanthanum/Iron Oxide Nanocomposite for Photo-Ultrafast Removal of Methyl Orange Dye and Toxicity Evaluation

[1]Rubina Nawaz, [1]Muhammad Asghar Jamal*, [2]Bushra Naseem, [1]Majid Munir, [3]Munawar Iqbal*
[1]*Department of Chemistry, Government College University Faisalabad, 38000 Pakistan.*
[2]*Department of Chemistry, Lahore College for Women University, Lahore, Pakistan.*
[3]*School of Chemistry, University of the Punjab, Lahore, Pakistan.*
asgharjamal@gcuf.edu.pk, munawar.chem@pu.edu.pk

(Received on 27th February 2025, accepted in revised form 13th May 2025)

Summary: In the present investigation, a lanthanum/iron oxide nanocomposite was prepared and employed for the removal of methyl orange dye. The nanocomposite was prepared via a co-precipitation method. Lanthanum nitrate hexahydrate ($La(NO_3)_3.6H_2O$) and iron nitrate hexahydrate ($Fe(NO_3)_2.6H_2O$) were precursor salts. The prepared nanocomposite was characterized using XRD, SEM, FTIR, EDX and UV/Vis spectroscopy. The average particle size measured by Scherrer's relation was in 15-20 nm range and particles showed the tendency of aggregates formation. The photocatalytic activity of the nanocomposite was evaluated against methyl orange (MO) dye (as a model organic pollutant) and up to 96% degradation of dye was achieved within 120 minutes of irradiation. The scavenging studies showed that •OH radical played a major role in MO dye degradation followed by h^+ and e^- species. The cytotoxicity of treated and untreated wastewater sample was evaluated by the *Allium cepa* assay. The root lengths and root count were recorded in the case of untreated, treated wastewater, positive control (methyl methanesulfonate) and negative control (distilled water) samples. The increase in root length and root count was observed to be 50% and 28.57% in the treated versus the untreated wastewater sample. The lanthanum/iron oxide nanocomposite also showed promising recyclability and reusability potential. The prepared lanthanum/iron oxide nanocomposite showed promising photocatalytic activity, which could have potential application for the remediation of dyes in the textile effluents.

Keywords: Lanthanum/iron oxide; Nanocomposite; Photocatalytic; Textile effluents

Introduction

Water pollution is one of the major factors relentlessly affecting the environment [1]. Industries such as leather, paper and textile are generating hundreds of tons of dyes per year. Industrial waste with excessive quantities of synthetic dyestuff, when directly discharged into water sources makes water substantially polluted [2-3]. The direct discharge of colored effluents into water bodies has adverse effects not only on human civilization but also obstructs the absorption of light essential for photochemical reactions in aquatic ecosystems [4]. Moreover, the toxicity of azo dyes even at a concentration of 0.001mg/L is perilous to microbes, plants and human life [5]. Hence, it is essential to remove dyes from wastewater before released into water bodies.

Removal of dyes is one of the major challenges as the majority of dyes are non-biodegradable [6]. Different physical and chemical methods have been employed for the elimination of pollutants from wastewater. Due to the chemical stability of synthetic dyes, the conventional techniques are ineffective in completely mineralizing the dyes [7]. For wastewater treatment, researchers are focused on using nanomaterial-based photocatalysts for the degradation of pollutants. Photocatalysis processes are inexpensive, environment-friendly and proficient for mineralization of contaminants [8-9]. In a photocatalytic process, a photon of energy equal to or higher than the band gap energy of a semiconductor oxide catalyst is employed [10]. The absorption of photons creates light-induced charge pairs as the electron jumps from the valence band of the catalyst to the conduction band. These photogenerated charge carriers facilitate redox reactions to decompose pollutants and the recombination of these charge pairs must be reduced for better improved catalytic activity of photocatalysts [11].

The nanoparticles like Cu, Co, Fe, Mn and V [12-15] due to mechanical, chemical, optical, and electronic properties [16-17] have gained much attention worldwide. However, to construct heterogeneous catalysts, lanthanides are considered ideal due to complex formation by using f orbitals with Lewis bases such as amines, aldehydes, alcohols and thiols [18]. Among nanostructured lanthanides, lanthanum oxide nanoparticles are very effective when

*To whom all correspondence should be addressed.

combined with metal oxides for the development of nanocomposite material [19]. Lanthanum quashes the recombination by trapping electrons to recombine with holes and improves the catalytic activity of photocatalysts [20]. Lanthanum-doped copper oxide nanoparticles were synthesized by the combustion technique for the degradation of methylene blue [21]. Lanthanum nanocomposites with different transition metal oxides were prepared for the photodegradation of methyl violet dye [22]. The La-doped CeO_2 nanoparticles were prepared to mineralize Rose Bengal dye [23].

Based on the aforementioned facts, the present research was designed to synthesize lanthanum/iron oxide nanocomposite by a simple, eco-friendly and inexpensive co-precipitation method. The prepared nanocomposite was characterized and its photocatalytic activity was evaluated against MO dye under UV light irradiation. Based on photocatalytic data, the dye degradation mechanism was proposed along the identification of free active species responsible for dye degradation. The cytotoxicity of the treated and untreated dye samples was performed using *Allium cepa* assay.

Experimental

Chemicals and reagents

Lanthanum nitrate hexahydrate ($La(NO_3)_3 \cdot 6H_2O$), iron nitrate hexahydrate ($Fe(NO_3)_2 \cdot 6H_2O$, sodium hydroxide and methanol were procured from Sigma Aldrich (Berlin, Germany). Methyl orange dye was purchased from Uni Chem. Chemical Reagents Co.; Ltd. Double-distilled water was used for the preparation of solutions. All the chemicals used during the experiment were of analytical research grade and were used as supplied.

Synthesis of lanthanum/iron oxide nanocomposite

The co-precipitation method was used for the synthesis of lanthanum/iron oxide nanocomposite. Lanthanum nitrate hexahydrate and iron nitrate hexahydrate were used as precursors of lanthanum and iron, respectively, and NaOH was used as a precipitant. The pre-weighed amount of lanthanum nitrate was dissolved in 250 mL of double-distilled water, whereas a 0.02 M aqueous solution of iron nitrate was prepared in 200 mL of water. Sodium hydroxide solution (0.2 M) was added dropwise to the suspension till the pH reached 11. The solution was agitated continuously at 70 °C for 7 hours until precipitates appeared. The collected precipitates were washed with acetone and ethanol and then dried in an oven at 85 °C. The dried residue was ground and calcined in a muffle furnace at 600 °C for 7 hours. Fig. 1 represents the steps involved in the synthesis of a nanocomposite.

Characterization of nanocomposite

Lanthanum/iron oxide nanocomposite was characterized using various techniques. Structure and average nanoparticle size were determined by XRD analysis (JDX-3532 (JEOL, Tokyo, Japan) diffractometer with Cu-Kα (λ = 1.5046 Å) radiation. For functional group identification, FTIR spectrophotometer (Perkin Elmer, Überlingen, Germany) analysis in 500 to 4000 cm^{-1} range was employed. A scanning electron microscope (SEM) with a cube compact model, Emcraft Seoul, South Korea, was used to examine the surface morphology of the nanocomposite. For optical property study, UV/Vis spectrophotometer (C-7200S Buxton, UK) was employed.

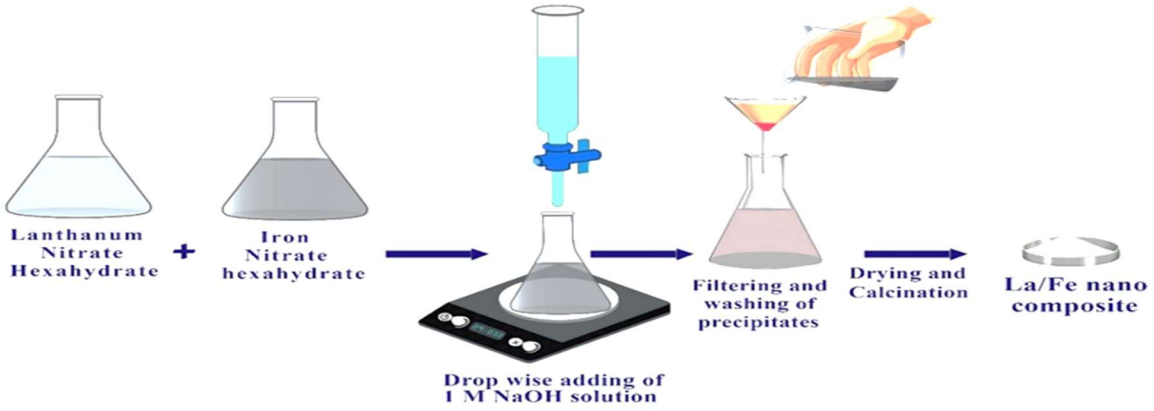

Fig. 1: Schematic presentation for the synthesis of lanthanum/iron oxide nanocomposite.

Photocatalytic procedure

The photocatalytic activity of the nanocomposite was evaluated against MO dye under UV light irradiation. For this, 0.5 g of catalyst was added to 500 mL of dye solution. The suspension was stirred for 30 minutes in the dark for adsorption-desorption equilibrium to be established between the dye and the catalyst. Afterwards, this suspension was irradiated with UV light with continuous stirring and 3 mL of samples from the suspension were collected at different intervals of time. The collected samples were centrifuged to remove the catalyst and absorbance was recorded at 464 nm using UV/Vis spectrophotometer (C-7200S Buxton, UK) and dye removal efficiency was estimated using the relation shown in Eq. 1. [24].

$$\text{Dye removal efficiency (\%)} = C_o\text{-}C_t/C_o * 100 \quad (1)$$

where C_o and C_t are the absorbance values before and after irradiation, respectively.

Cytotoxicity study using Allium cepa

Textile wastewater samples were collected in pre-cleaned gallons from Haaris Dyes and Chemicals, Faisalabad. The samples were filtered to remove particulates and stored at 4 °C before use. Healthy onion (*Allium cepa*) bulbs of similar size and weight were selected and pre-cleaned by removing loose outer scales and dried roots. The bulbs were placed in distilled water for 24 hours to stimulate root growth. The bulbs were then transferred to separate beakers containing untreated (before treatment) and treated wastewater samples (treated at conditions used for dye solution treatment). A positive and negative control group was maintained in distilled water and methyl methanesulfonate (10 mg/L) solution. The exposure lasted for 48 hours at room temperature under dark conditions to prevent interference from light-induced reactions. After exposure, the root lengths of five randomly selected bulbs from each group were measured using a scale. The average root length was calculated to assess the cytotoxic effects of wastewater. The number of roots was also counted for the bulbs exposed to untreated (before treatment) and treated (after treatment) wastewater, along with control groups. The root length and root number data were averaged and reported as ±SD of five replicates for each treatment.

Recyclability analysis

The recycling and reusability of La/iron oxide nanocomposite for MO dye was studied, which is useful for practical applications. Five successive cycles were run to assess the recycling and reusability of La/iron oxide nanocomposite for MO dye. For this, 0.5 g of catalyst was added to 500 mL of dye solution, stirred in the dark for 30 min and irradiated under UV light for 120 minutes. For dye residual concentration analysis and to recover the catalyst, samples were centrifuged, absorbance was recorded and dye degradation was estimated using Eq. 1. After each cycle, La/iron oxide nanocomposite was collected, dried at 50 °C and subjected to the next cycle.

Scavenging studies

The scavenging studies were performed. The dye degradation run was conducted in the presence of scavengers, i.e., 2-propanol ($^{\bullet}OH$ scavenger), EDTA (h^+ scavenger), $AgNO_3$ (e^- scavenger) and without any scavenger, which was used as a control. The impact of each scavenger on photocatalytic efficiency was analyzed to determine the MO dye degradation in the presence of the scavenger in comparison to the control (without the scavenger).

Results and Discussion

X-ray diffraction analysis (XRD)

The crystallographic and structural determination of the La/iron oxide nanocomposite was performed using a powder X-ray diffractometer. The XRD was performed at room temperature in an angle range of 20° to 70° and response is represented in Fig. 2. The appearance of diffraction peaks in the XRD pattern indicated the crystal structure of lanthanum/iron oxide. These findings are in agreement with the ICCD card No. 00-002-0688 for lanthanum oxide [25], while the ICCD card No.19-0629) for iron oxide [26], respectively. The peaks observed at 2θ = 26° (002), 28° (100) and 30° (101) indicated a hexagonal phase [27]. The synergistic effect of lanthanum and iron oxides in the nanocomposite is evidenced by the peaks at 2θ values of 40° (102) and 48° (110) [28]. The appearance of peaks at 2θ = 51° (101) and 55° (111) [29] confirmed the formation of binary nanocomposite. The sharpness of peaks specified that the synthesized lanthanum/iron oxide nanocomposite was a crystalline material. The average crystallite size of the nanocomposite was calculated by the Debye-Scherrer relation shown in Eq. 2.

$$D = 0.89/\beta Cos\theta \quad (2)$$

where D is the average crystallite size, K is a constant, wavelength (λ) 1.5406 is in A, while full-width half maxima (FWHM) β is in radians [30]. The average crystallite size of nanoparticles of the composite was in 15-20 nm range.

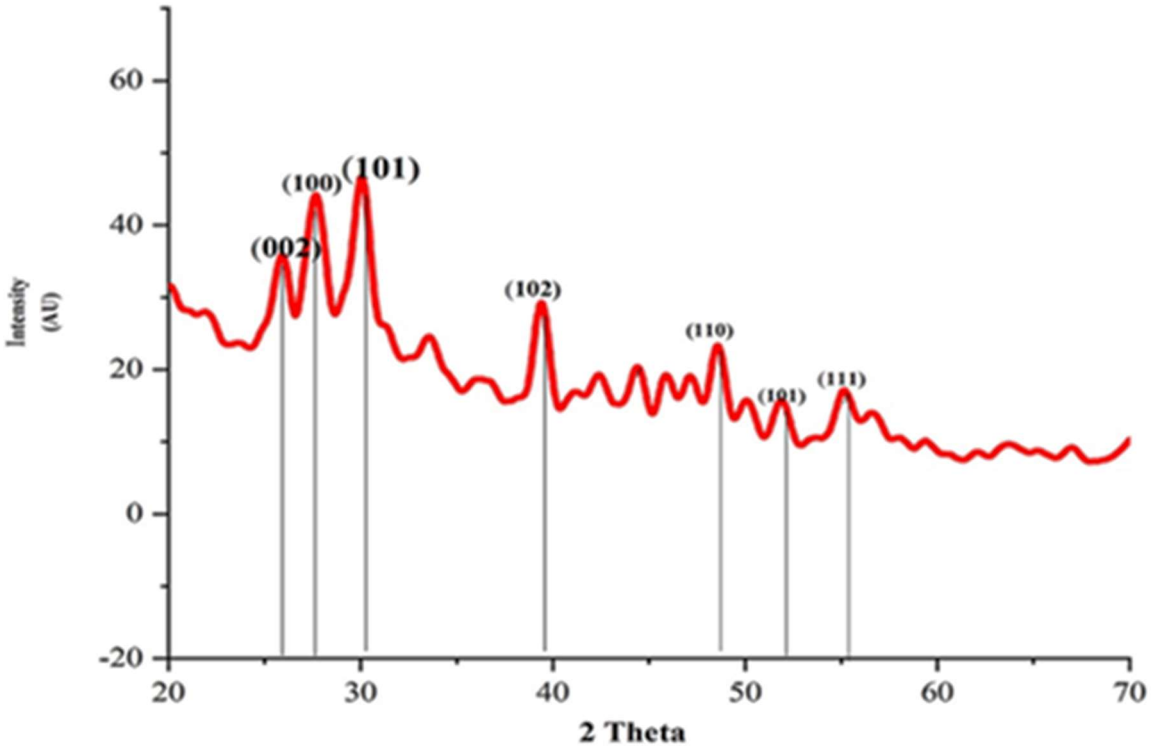

Fig. 2: X-ray diffraction pattern of La/iron oxide nanocomposite.

Surface Morphological Analysis

The surface morphology of the La/iron oxide nanocomposite was examined by scanning electron microscopy analysis and the responses thus observed are depicted in Fig. 3. The SEM analysis revealed the formation of aggregates in the binary nanocomposite. The SEM image of the La/iron oxide nanocomposite reveals a rough, porous, and agglomerated morphology. The nanocomposite appears to consist of irregularly shaped clusters, likely due to the strong interaction between La and iron nanoparticles. The presence of voids and rough textures suggests a high surface area, which is beneficial for photocatalytic applications by enhancing dye adsorption and active species interaction. The individual particles are in nano size but have formed agglomerates, a common feature in metal oxide-based nanocomposites. SEM images evidenced lanthanum/iron oxide composite is a crystalline material with the presence of iron particles on the lanthanum surface to form a nanocomposite with a heterogeneous surface to assist in the catalysis process.

Elemental composition analysis

The elemental composition of the La/iron oxide nanocomposite was determined by EDX, as shown in Fig. 4. The EDX analysis the La/iron oxide nanocomposite confirms the presence of elements, i.e., oxygen (O), iron (Fe), and lanthanum (La), indicating successful synthesis of the composite material. A strong oxygen peak appears at 0.52 keV with high intensity, affirming the presence of oxygen in the prepared material. Iron is identified through its characteristic peaks at 0.70 keV, 6.40 keV (prominent peak) and 7.06 keV (weak peak), which confirm its presence in the nanocomposite. Lanthanum is observed through multiple peaks: a low-energy peak at 0.83 keV, stronger peaks at 4.65 keV and a moderate intensity peak at 5.02 keV, indicating successful incorporation of La into the iron oxide matrix. The clear and distinct nature of these peaks, along with the absence of signals of others elements revealed the high purity of the sample and hence the EDX data thus validates the composition of La/iron oxide nanocomposite.

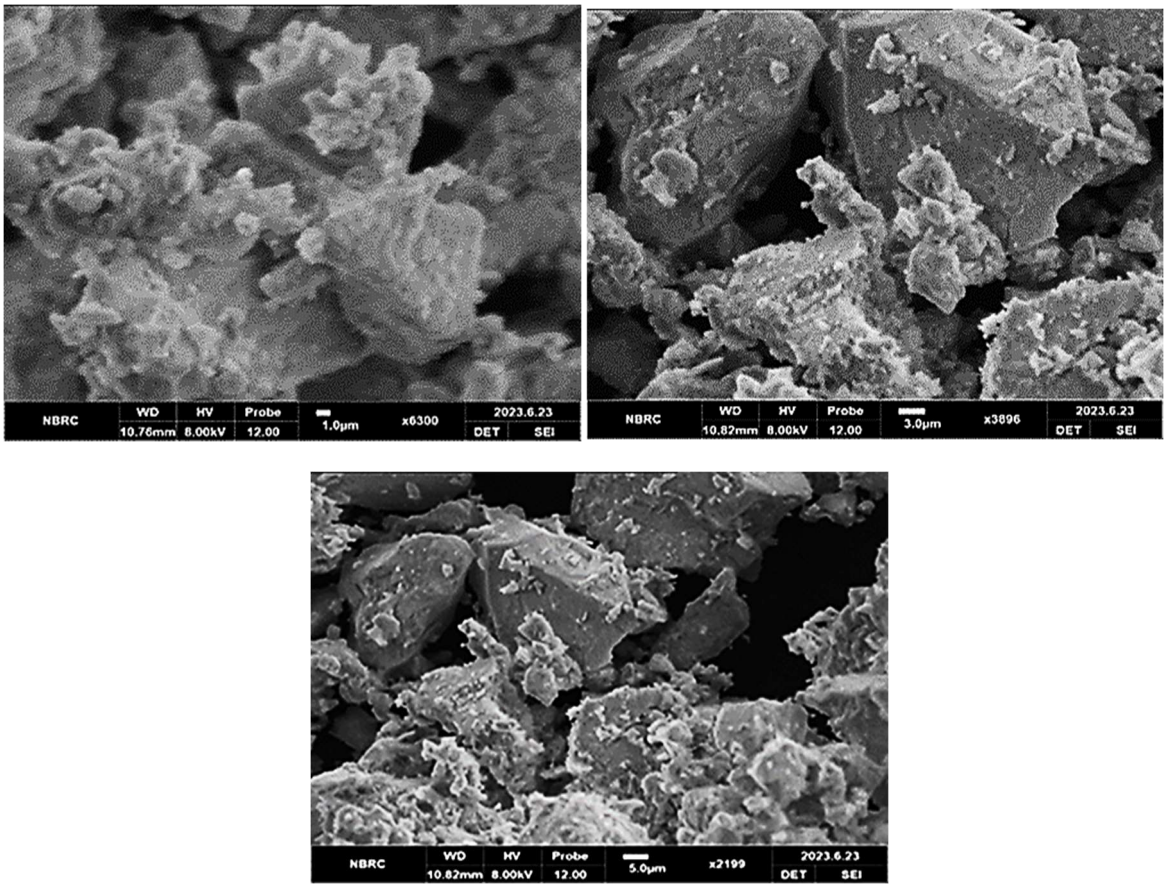

Fig. 3: SEM images of La/iron oxide nanocomposite at different resolutions.

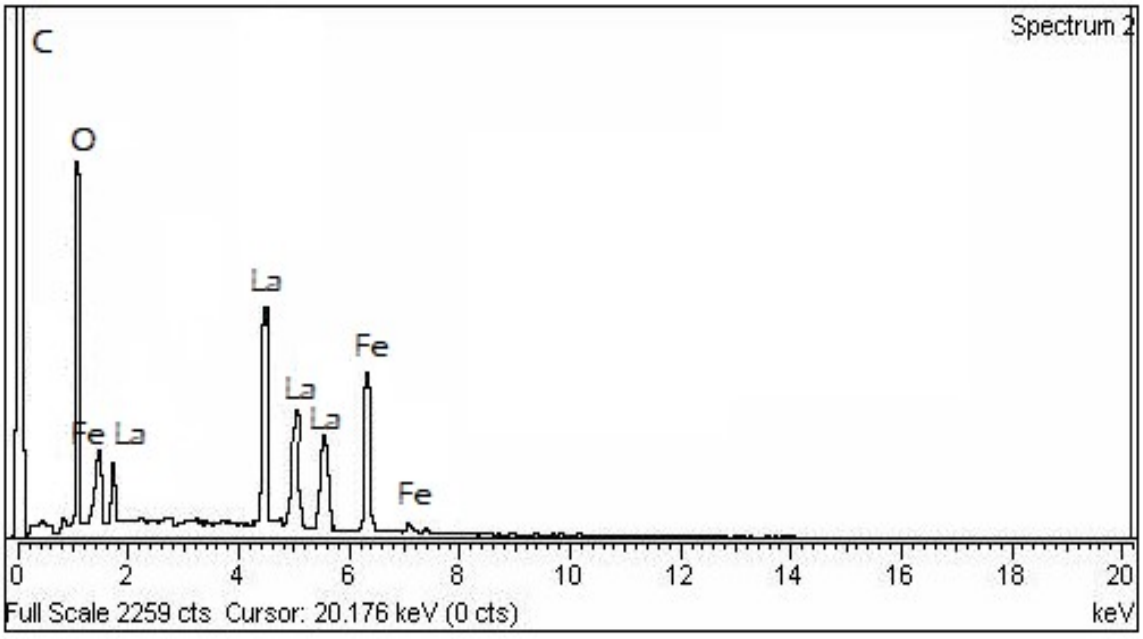

Fig. 4: EDX spectrum for La/iron oxide nanocomposite.

FTIR Analysis

Fourier transform infrared analysis was employed for the identification of functional groups and the response thus observed is presented in Fig. 5. The peaks observed at 3809 cm^{-1}, 1507 cm^{-1}, 1459 cm^{-1} and 650 cm^{-1}. The peak at 3809 cm^{-1} corresponds to the presence of stretching vibrational modes in the hydroxyl group of H_2O molecules being adsorbed on the catalyst surface, whereas the peaks at 1507 cm^{-1} and 1459 cm^{-1} shows the existence of asymmetric stretching of the N-O that might be due to nitrate and other impurity in the prepared sample [31-32]. The metal-oxygen bond in the nanocomposite is confirmed by a peak at 855 cm^{-1} and 650 cm^{-1} for vibrational modes in La–O and Fe–O, respectively [33].

UV/Vis spectroscopic analysis

A UV/Visible spectrophotometer was used to study the optical properties of the nanocomposite. UV/Vis spectrum for the composite is shown in Fig. 6. The optical behavior of the nanocomposite is studied to determine the absorption wavelength of the photocatalyst material. Absorption wavelength determines the difference between the energy band gap of the incident photon and the photocatalyst. In the La/iron oxide nanocomposite photocatalyst absorption wavelength was found near the UV region of the sunlight spectrum. Band gap measurements were done by Tauc's equation Eq. 3. [34].

$$\alpha = A(hv\text{-}E_g)^{n}/hv \qquad (3)$$

In this equation, α is the coefficient of absorption, hv represents the energy of the photon, A is a constant, E_g is the band gap energy, whereas n is a constant with a ½ value for direct band-gap semiconductor oxides [35]. The band gap values for the La/iron oxide nanocomposite were found to be 5.01 eV, which revealed that the La/iron oxide nanocomposite is active under UV light for effective photocatalytic application and same was observed during photocatalytic experiment for the degradation of methyl orange dye. The obtained outcomes are according to the results of photocatalytic reactions in which light-induced electron-hole charge pairs noticeably participate in a redox reaction to decompose the organic pollutants [36].

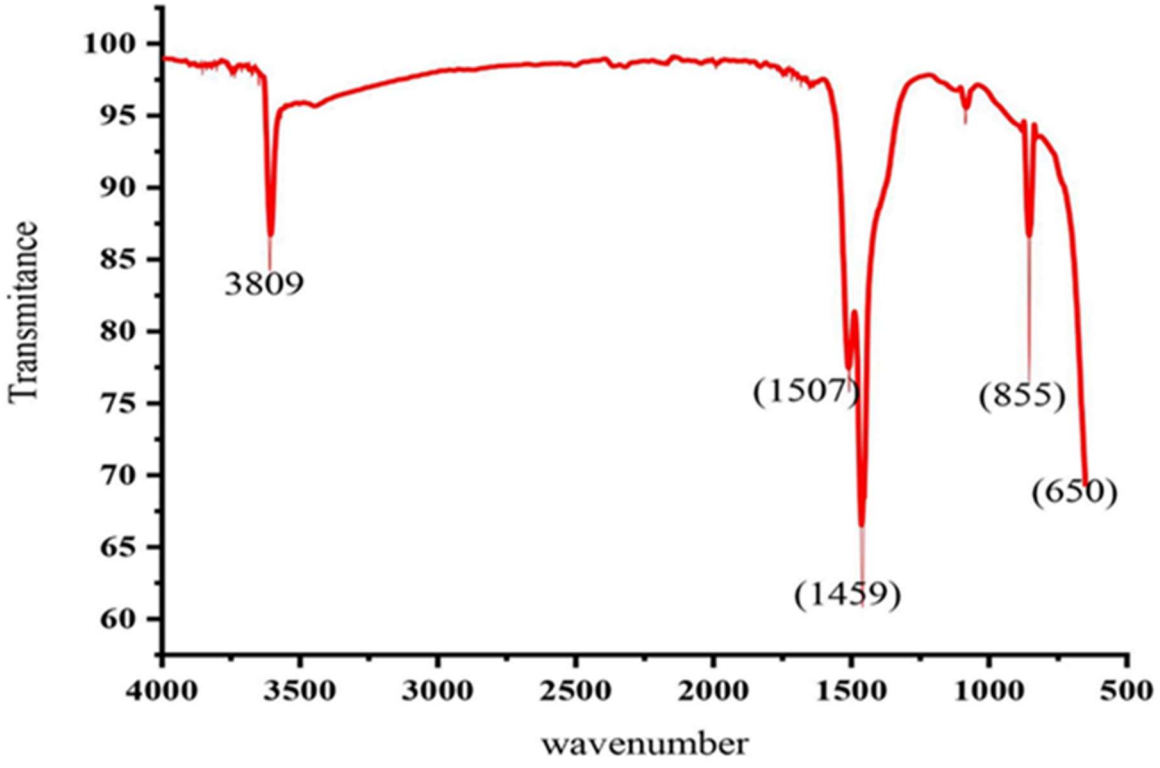

Fig. 5: FTIR spectrum of the La/iron oxide nanocomposite.

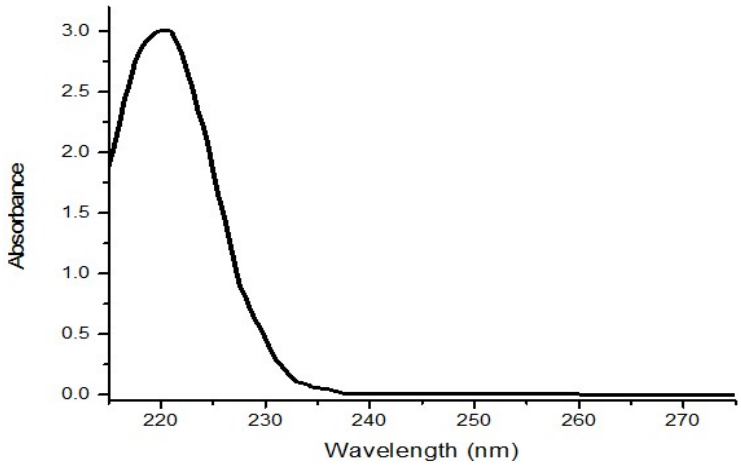

Fig. 6: UV/Vis spectra of La/iron oxide nanocomposite.

Photocatalytic Activity of La/iron oxide nanocomposite

The present study focuses on the synthesis of the La/iron oxide nanocomposite for elution of MO dye under UV light irradiation and the nanocomposite showed enhanced photocatalytic activity. The MO dye degradation using nanocomposite in 120 minutes is depicted in Table 2 and corresponding graphical presentation in Fig. 7. The MO dye degradation was recorded to be 96% in 120 minutes of irradiation, which is sinical higher than the reported degradation of dyes using related photocatalysts [37-38]. Jiang et al., 2016 [37] studied the synthesis of iron oxide nanoparticles, which presented 86% photocatalytic activity against methyl orange dye. Whereas Zainab et al., 2021 [38] employed La_2O_3 nanoparticles for the degradation of 4-chlorophenol, which revealed a 92% degradation. The enhanced photocatalytic activity of the La/iron oxide nanocomposite is attributed to improved charge separation efficiency and reduced electrons-holes recombination. Additionally, the presence of La ions enhances light absorption and provides active sites for the photocatalytic reactions. A nanocomposite photocatalyst material has the enhancement of surface oxygen defects than individual metal oxide. The increased concentration of surface oxygen defects holds photogenerated electrons-holes separate to make them available for pollutant decomposition. This delayed recombination of charge carriers increases their availability for oxidation-reduction reaction and increases photocatalytic activity for the decomposition of dye [39]. A comparison of degradation efficiency with reported similar studies is given in Table 2. The photocatalytic degradation curve of MO dye is represented in Fig. 8(a), whereas the plot for absorbance of dye is shown in Fig. 7(b) and percentage degradation in the presence of La/iron oxide photocatalyst is displayed in Fig. 7(c). The distinctiveness of the present research is the preparation of La/Fe_3O_4 nanocomposite with improved photocatalytic activity. The mechanism of the photocatalytic degradation of dye is presented in Fig. 8 and the chemical reactions involved are depicted in Eqs. 4-9. Upon irradiation with light energy, the photocatalyst absorbs photons, exciting electrons (e^-) from the valence band (VB) to the conduction band (CB), leaving behind holes (h^+) in the VB. The photogenerated electrons in the CB reduce oxygen (O_2) molecules to form superoxide radicals ($O_2^{\bullet-}$), which further react with water to produce hydroperoxyl ($HOO^\bullet$) and hydroxyl ($HO^\bullet$) radicals. Meanwhile, the holes (h^+) in the VB oxidize water molecules to produce additional hydroxyl radicals ($^\bullet OH$). These highly reactive species ($^\bullet OH$ and $O_2^{\bullet-}$) attack and degrade the MO dye into water, carbon dioxide, and inorganic ions, effectively removing the dye from the solution.

La/iron oxide + Irradiation → La/Fe_3O_4 (e^-)(CB) + La/Fe_3O_4 (h^+) (VB) (4)

La/Fe_3O_4 (e^-) + O_2 → $O_2^{\bullet-}$ (5)

La/Fe_3O_4 (h^+) + H_2O → $^\bullet OH$ + La/Fe_3O_4 (6)

$O_2^{\bullet-}$ + H_2O → $^\bullet OOH$ + OH^- → H_2O_2 (7)

H_2O_2 + $O_2^{\bullet-}$ → $^\bullet OH$ + OH^- (8)

Dye + $^\bullet OH$ + $O_2^{\bullet-}$ → H_2O + CO_2 + inorganic ions (9)

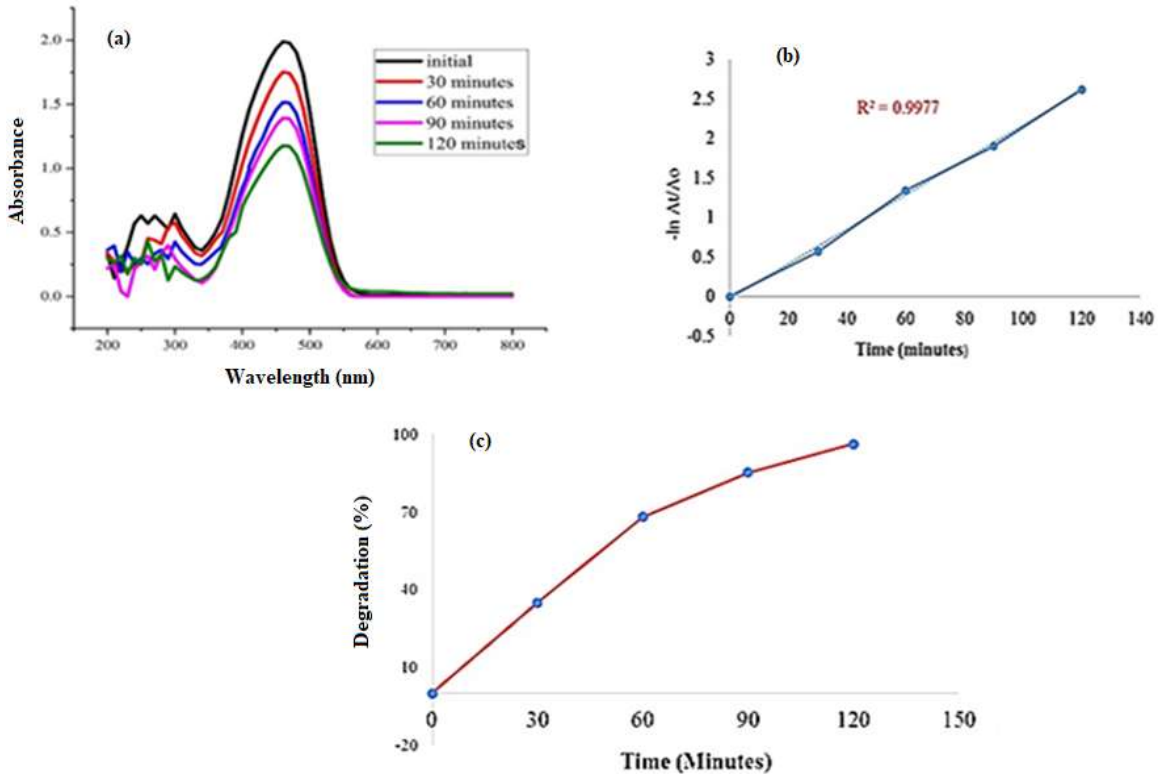

Fig. 7: (a) Degradation of methyl orange dye in the presence of La/iron oxide nanocomposite, (b) Plot for the natural logarithm of MO absorbance vs time and (c) Percentage photocatalytic degradation of methyl orange dye.

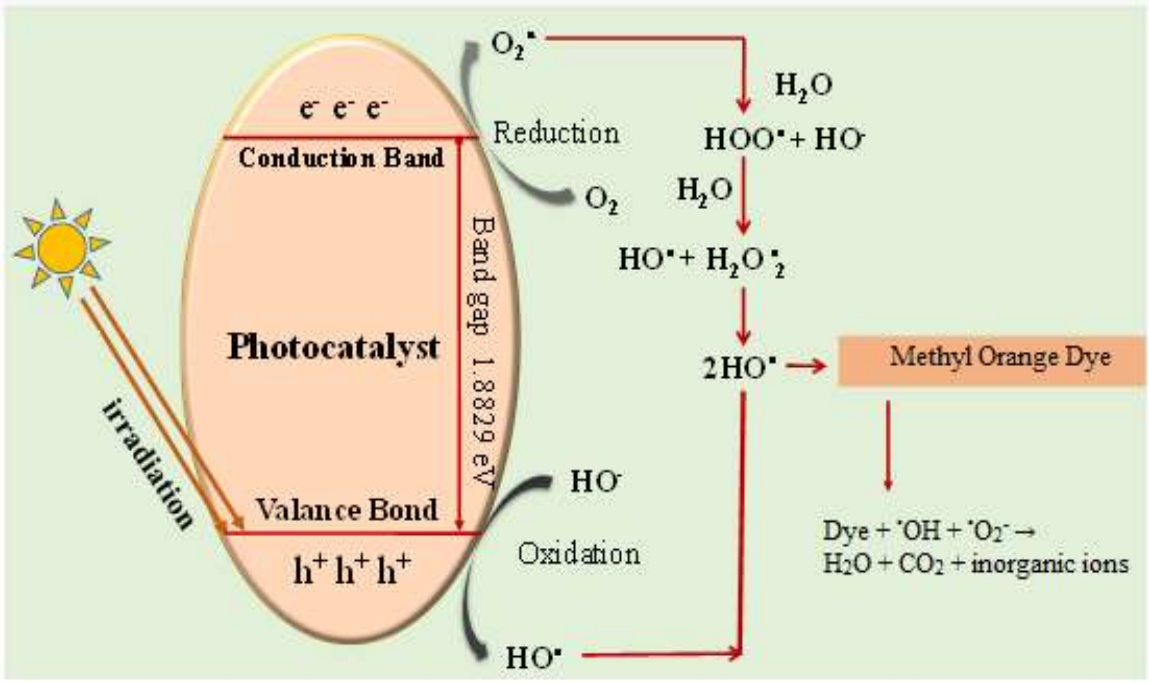

Fig. 8: Proposed mechanism for the removal of dye over La/iron oxide (photocatalyst) nanocomposite.

Cytotoxicity Analysis

The *Allium cepa* test is a commonly employed bioassay to evaluate the toxicity of textile wastewater due to its simplicity, affordability, and reliability. This method uses onion (*Allium cepa*) bulbs to examine the cytotoxic, genotoxic, and mutagenic effects of contaminants in wastewater. The test assesses the impact of toxic substances on cell division by analyzing root growth and mitotic activity in the meristematic cells of onion root tips. Indicators such as reduced root length or a lower mitotic index reflect cytotoxic effects. In this study, the cytotoxicity of textile wastewater was analyzed both before and after treatment, with the results illustrated in Fig. 9. Results revealed that the RL and RC values are relatively low in the case of untreated textile, indicating that untreated textile wastewater exhibits cytotoxic effects, likely due to the presence of toxic contaminants like dyes inhibiting root growth and cell division. On the other hand, in the treated wastewater, both RL and RC, increases significantly compared to the untreated sample. The root lengths were recorded to be 5, 10, 12 and 3 (cm) in case of untreated, treated wastewater sample, positive control (methyl methanesulfonate, 10 mg/L) and negative control (distilled water), respectively. The increase in root length was 50% in comparison to untreated wastewater sample. While the root counts were recorded to be 10, 14, 18 and 5 for untreated, treated wastewater sample, positive control (methyl methanesulfonate, 10 mg/L) and negative control (distilled water), respectively. The increase in root count was 28.57% versus untreated wastewater sample. This suggests that the photocatalytic treatment effectively reduced the toxicity, allowing better root growth and higher mitotic activity. The positive and negative controls show the validity of the test for evaluation of cytotoxicity because the highest and lowest RL and RC values were observed for the positive and negative controls, respectively. Hence these findings revealed that the photocatalytic treatment of textile wastewater significantly reduces cytotoxicity, as shown by the improved root growth and root count. The treated sample shows intermediate values between the untreated wastewater and the positive control, suggesting that while the treatment improves conditions, some residual toxicity may still be present. The findings demonstrated a significant reduction in toxicity after treatment, highlighting the effectiveness of the photocatalytic process for the remediation of toxic dyes in the effluents.

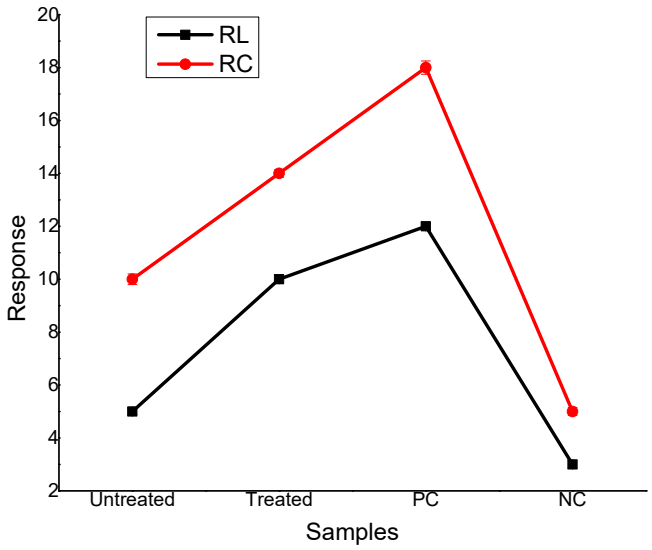

Fig. 9: Cytotoxicity of the profile of textile wastewater (treated and untreated). RC = root count, RL = root length, NC = negative control and PC = positive control. PC and NC were methyl methanesulfonate (10 mg/L) and negative control distilled water, respectively).

Table-2: Comparison of photocatalytic efficiency of La/Fe_3O_4 nanocomposite with reported work.

Nanocomposite	Pollutant Degraded	Reaction time (minutes)	Degradation Efficiency	References
La-doped Molybdenum oxide	Methyl orange	150	80 %	[40]
Lanthanum-bismuth oxide	Methylene Blue	120	81.32 %	[41]
La-doped zinc oxide	Methyl Orange	150	85.86 %	[42]
Iron oxide	Sunlight	180	87%	[43]
α-iron oxide	Methylene Blue	120	78%	[44]
Lanthanum/iron Oxide	Methyl Orange	120	96 %	Present study

Recyclability and scavenging studies

For recyclability and reusability, five successive cycles of photocatalytic activity were runs. The data represents the degradation efficiency (%) of a dye over successive cycles of photocatalytic activity, was declined slightly (Fig. 10). The degradation efficiency gradually declines with increasing cycles, indicating a reduction in the catalytic performance of the material over repeated use. In cycle I, the degradation efficiency was above 96%, which decreased slightly in cycle II and cycle III but remained above 94%. In cycle V, the degradation efficiency falls to around 92.5%, showing a decline in photocatalytic performance and this decline was 3.5% versus cycle I. The reason to the decline in photocatalytic activity might be the deactivation of active sites of the surface of the catalyst and the catalyst may undergo structural modifications over repeated use. The loss of active elements (e.g., La or iron oxide) from the nanocomposite and the intermediate species or residual dye may also block the active sites on the surface of the catalyst and resultantly, the efficiency was reduced. However, after cycle V, the efficiency was quite promising versus cycle I, suggesting that the catalyst retains substantial activity. Future studies could focus on regeneration strategies to improve the reusability of La/iron oxide nanocomposite.

The contribution of free active species was evaluated by performing the dye degradation in the presence of scavengers, which scavenge the free active species and the data thus obtained were used to identify the role of individual free active species in the degradation of dye by La/iron oxide nanocomposite. For this, 2-propanol, EDTA and $AgNO_3$ scavenging agents were employed. The 2-propanol is a scavenger of $^{\bullet}OH$ radical, while EDTA scavenges the h^+ and $AgNO_3$ scavenges the e^-. The dye degradation by the La/iron oxide nanocomposite was recorded to be 96% without using a scavenging agent (Fig. 11). In the presence of scavenging agents, the dye degradation was reduced significantly, which was reduced in the following order for 2-propanol > EDTA > $AgNO_3$. The dye degradation was reduced to 26.8% in the presence of 2-propanol, while it was 48.2% in the case of EDTA and 63.7% in the case of $AgNO_3$. The results showed that the $^{\bullet}OH$ radical played a major role for the eradication of dye, followed by h^+ and e^-. These findings demonstrate that $^{\bullet}OH$ radicals are the predominant active species responsible for dye degradation, followed by h^+ and e^-. The decline in dye degradation in the presence of scavengers confirms the crucial role of these species in the photocatalytic process of dye using the La/Fe_2O_3 nanocomposite.

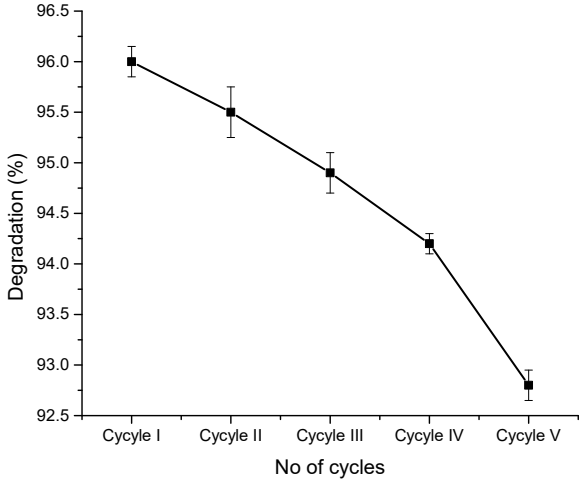

Fig. 10: Reusability and recycling analysis for the degradation of methyl orange dye using La/Fe_2O_3 nanocomposite.

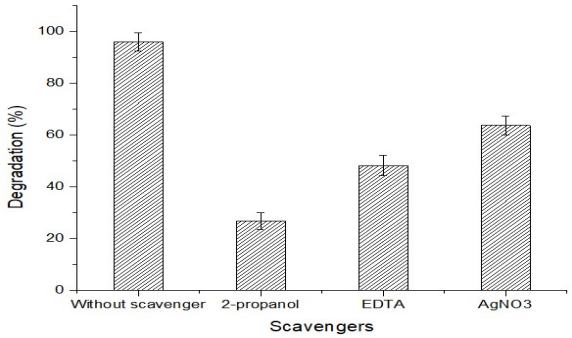

Fig. 11: Methyl orange dye degradation (%) with and without scavengers for the analysis of free active species.

Conclusions

The La/iron oxide nanocomposite was successfully synthesized via the co-precipitation method and thoroughly characterized using XRD, SEM, EDX, FTIR, and UV/Vis spectroscopy. XRD analysis confirmed the formation of a well-crystallized nanocomposite with an average crystallite size of 15–20 nm. The material demonstrated excellent photocatalytic performance, achieving 96% degradation of methyl orange dye within 120 minutes under UV light irradiation. Moreover, cytotoxicity evaluation through the *Allium cepa* assay revealed a significant reduction in toxicity of the treated textile wastewater, with a 50% increase in root length and a 28.57% rise in root count compared to untreated samples. The nanocomposite also exhibited promising recyclability and reusability, indicating its potential for sustainable applications. The La/iron oxide nanocomposite emerges as a highly efficient and reusable photocatalyst for the degradation of textile dyes, offering both environmental and practical benefits. Future research should focus on optimizing its activity under visible light, scaling up the synthesis process for industrial applications, and exploring its effectiveness against a broader range of organic pollutants. Additionally, detailed mechanistic studies and long-term toxicity assessments will further validate its safety and efficiency for wastewater treatment applications.

References

1. D. Kavaz, Effective methylene dye removal from contaminated water using zinc oxide nanoparticles fabricated from the green synthesis of *Laurus nobilis* leaf, *J. Chem. Soc. Pak.,* **46**, 535 (2024).
2. R. Simiyu, S. Apollo and G Muriithi, A review of municipal wastewater disinfection using advanced oxidation processes, *J. Chem. Soc. Pak.,* **46**, 600 (2024).
3. F. Shokry, M. El-Gedawy and SA Nosier, Optimizing photocatalytic degradation of methyl violet dye in a recirculating slurry-type reactor, *Result. Chem.,* **13**, 101980 (2025).
4. I. M. Banat, P. Nigam and D. Singh, Microbial decolorization of textile-dye containing effluents: a review, Bioresour. Tech., **58**, 217 (1996).
5. K. N. Riaz, N. Yousaf and M. Bilal Tahir, Facile hydrothermal synthesis of 3D flower-like La-MoS_2 nanostructure for photocatalytic hydrogen energy production, *Int. J. Energy. Res.,* **43**, 491 (2019).
6. A. R. A. Giwa, I. A. Bello and A. B. Olabintan, Kinetic and thermodynamic studies of Fenton oxidative decolorization of methylene blue, *Helion,* **6**, e04454 (2020).
7. A. Kheyrandish, M. Mohseni and F. Taghipour, Development of a method for the characterization and operation of UV-LED for water treatment, *Water Res.,* **122**, 570 (2017).
8. M. Saquib, M. A. Tariq and M Faisal, Photocatalytic degradation of two selected dye derivatives in aqueous suspensions of titanium dioxide, *Desalination,* **219**, 301 (2008).
9. M. Ahmaruzzaman, Biochar based nanocomposites for photocatalytic degradation of emerging organic pollutants from water and wastewater, *Mater. Res., Bull.* **140**, 111262 (2021).
10. J. Zhang, D. Fu and Y. Xu, Optimization of parameters on photocatalytic degradation of chloramphenicol using TiO2 as photocatalyist by response surface methodology, J. Environ. Sci., **22**, 1281 (2010).
11. Y. Lee, J. Suntivich and K. J. May, Synthesis and activities of rutile IrO_2 and RuO_2 nanoparticles for oxygen evolution in acid and alkaline solutions, *J. Phys. Chem. Lett.,* **3**, 399 (2012).
12. G. Colon, M. Maicu and M. C. Hidalgo, Cu-doped TiO_2 systems with improved photocatalytic activity, *Appl. Catal. B. Environ.,* **67**, 41 (2006) 41.
13. B. Hamal and K. J. Klabunde, Valence state and catalytic role of cobalt ions in cobalt TiO_2 nanoparticle photocatalysts for acetaldehyde degradation under visible light, *J. Phys. Chem. C,* **115**, 17359 (2011).
14. F. Mazille, T. Schoettl and C. Pulgarin, Synergistic effect of TiO_2 and iron oxide supported on fluorocarbon films. Part 1: Effect of preparation parameters on photocatalytic degradation of organic pollutant at neutral pH, *Appl. Catal. B.* Environ., **89**, 635 (2009).
15. P. Sathishkumar, S. Anandan and P. Maruthamuthu, Synthesis of Fe^{3+} doped TiO_2 photocatalysts for the visible assisted degradation of an azo dye, Colloids Surf. A, **375**, 231 (2011).

16. Q. R. Deng, X. H. Xia and M. L. Guo, Mn-doped TiO_2 nanopowders with remarkable visible light photocatalytic activity, Mater. Lett., **65**, 2051 (2011).
17. K. R. Reyes-Gil, Y. Sun and E. Reyes-Garcia, Characterization of photoactive centers in N-doped In_2O_3 visible photocatalysts for water oxidation, *Phys. Chem. C,* **113**, 12558 (2009).
18. K. T. Ranjit, I. Willner and S. H. Bossmann, Lanthanide oxide doped titanium dioxide photocatalysts: effective photocatalysts for the enhanced degradation of salicylic acid and *t*-cinnamic acid, J. Catal., **204**, 305 (2001).
19. S. P. Jiang, Development of lanthanum strontium cobalt ferrite perovskite electrodes of solid oxide fuel cells, *Int. J. Hydrog Energy,* **44**, 7448 (2019).
20. H. Kochkar**,** M. Aouine and A. Ghorbel, shape-controlled synthesis of silver and palladium nanoparticles using β-cyclodextrin, *J. Phys. Chem. C,* **115**, 23 (2011).
21. J. D. Rodney, S. Deepapriya and P. A. Vinosha, Photo-Fenton degradation of nano-structured La doped CuO nanoparticles synthesized by combustion technique, *Optik,* **161**, 204 (2010)
22. M. A. Subhan, A. M. M. Fahim and P. C. Saha, Structural study, photoluminescence and photocatalytic properties of $La_2O_3 \cdot Fe_3O_4 \cdot ZnO$, $AgO \cdot NiO \cdot ZnO$ and $La_2O_3 \cdot AgO \cdot ZnO$ nanocomposites. *Nano-Struct. Nano-Object,* **10**, 30 (2017).
23. S. Chahal, S. Singh and A. Kumar, Vacuum Oxygen-deficient lanthanum doped cerium oxide nanoparticles for potential applications in spintronics and photocatalysis, *Vacuum***, 177,** 109395 **(**2020).
24. N. Zhang and F. Zeng, Characterization, activity and mechanisms of a visible light driven photocatalyst: Manganese and iron co-modified TiO_2 nanoparticles, *Russ. J. Phys. Chem.,* **85**, 1825 (2011).
25. H. Katsui and N. Kondo, Preferred orientations and microstructures of lanthanum phosphate films prepared via laser chemical vapor deposition, *J. Cryst. Growth*, **519**, 46 (2021).
26. M. Zakirove, M. P. Semen'Ko and O. A. Korotchenkov, A simple sonochemical synthesis of nanosized ZnO from zinc acetate and sodium hydroxide, *J. Nano Electron. Phys.,* **10**, 5 (2018).
27. V. J. Mane, D. B. Malavekar and S. B. Ubale, Binder free lanthanum doped manganese oxide @ graphene oxide composite as high energy density electrode material for flexible symmetric solid state supercapacitor, *Electrochim. Acta,* **335**, 135613 (2020).
28. H. Tinwala, D. V. Shah and J. Menghani, Synthesis of $La_2Ce_2O_7$ nanoparticles by co-precipitation method and its characterization, *J. Nanosci. Nanotechnol.,* **14**, 6072 (2017).
29. A. Sescu, M. Harja and L. Favier, Zn/La mixed oxides prepared by co-precipitation: Synthesis, characterization and photocatalytic studies, Materials, **13**, 4916 (2020).
30. A. Manikandan, E. Manikandan and B. Meenatchi, Rare earth element (REE) lanthanum doped zinc oxide (La: ZnO) nanomaterials: Synthesis structural optical and antibacterial studies, *J. Alloy. Compound.,* **723**, 1155 (2017).
31. S. Yan, S. O. Salley and K. Y. S. Ng, Simultaneous trans esterification of unrefined or waste oils over $ZnO\text{-}La_2O_3$ catalysts, Appl. Catal. A: Gen., 353, 203 (2009).
32. O. M. Alfano, D. Bahnemann and A. E. Cassano, Photocatalysis in water environments using artificial and solar light, *Catal. Today,* **58**, 199 (2000).
33. X. Yang, C. Cao and L. Erickson, Synthesis of visible-light-active TiO_2-based photocatalysts by carbon and nitrogen doping, *J. Catal.,* **260**, 128 (2008).
34. S. Higashimoto, Titanium-dioxide-based visible-light-sensitive photocatalysis: Mechanistic insight and applications, *Catalysts,* **9**, 128 (2019).
35. D. Chen, Z. Jiang and J. Geng, Carbon and nitrogen co-doped TiO_2 with enhanced visible-light photocatalytic activity, *Ind. Eng. Chem. Res.,* **46**, 2741 (2007).
36. D. Chen, Y. Cheng and N Zhou, Photocatalytic degradation of organic pollutants using TiO_2-based photocatalysts: A review, *J. Clean. Product.,* **268,** 121725 (2020).
37. I. Ahmad, M. A. Jamal and M. Iftikhar, Lanthanum-zinc binary oxide nanocomposite with promising heterogeneous catalysis performance for the active conversion of 4-nitrophenol into 4-aminophenol, *Coatings,* **11**, 537 (2021).
38. I. Bibi, U. Ali and S. Kamal, Synthesis of $La_{1-x}Co_xFe_{1-y}CryO_3$ nano crystallites for enhanced ferroelectric, magnetic and photocatalytic properties, *J. Mater. Res. Technol.,* **9**, 12031 (2020).
39. G. Zeinab, M. Moussavi and S Jorfi, Enhanced phpotocatalytic degradation of 4 chlorophenol using lanthanum oxide nanoparticles under UVC/Vis irradiation, *J. Nanostruct.,* **1**, 165 (2021).
40. M. A. Subhan, T. Ahmed and N. Uddin, Synthesis, characterization, PL properties, photocatalytic and antibacterial activities of nano multi-metal oxide $NiO\cdot CeO_2\cdot ZnO$, *Spectrochim. Acta A. Mol. Biomol. Spectroscopy,* **5**, 824 (2015).
41. T. Abraham, S. Kannan and R. N. Priyanka, A novel lanthanum and bismuth based self-cleaning nanocomposite for organic pollutants, AIP Conference Proceedings, AIP Publishing (2020).

42. R. J. Sayyad and S. R. Gadale, Synthesis, characterization and photocatalytic activity of nanocrystalline Lanthanum doped molybdenum oxide, *J. Adv. Sci. Res.,* **13**, 153 (2022).
43. I. Tahir and M Sohaib, Synthesis of novel lanthanum-doped zinc oxide nanoparticles and their applications for waste water treatment, *Appl. Nanosci.,* **11**, 2599 (2021).
44. H. Inam, U. Fatima and S. Shahid, Nanotheranostic fabrication of iron oxide for rapid photocatalytic degradation of organic dyes and antifungal potential, *J. Saudi Chem. Soc.,* **27**, 101689 (2023).
45. M. B. Goudjil, H. Dali and S. Zighmi, Photocatalytic degradation of methylene blue dye with biosynthesized Hematite α-Fe_2O_3 nanoparticles under UV-irradiation, *Desalinat. Water Treat.,* **317**, 100079 (2024).